Fractal characterization of multiscale fracture network distribution in dolomites : outcrop analogue of subsurface reservoirs

Pavičić, Ivica; Duić, Željko; Vrbaški, Anja; Dragičević, Ivan

fractal and fractional

MDPI

Article

Fractal Characterization of Multiscale Fracture Network Distribution in Dolomites: Outcrop Analogue of Subsurface Reservoirs

Ivica Pavičić, Željko Duić *, Anja Vrbaški and Ivan Dragičević

Faculty of Mining, Geology and Petroleum Engineering, University of Zagreb, 10000 Zagreb, Croatia; ivica.pavicic@rgn.unizg.hr (I.P.); anja.vrbaski@rgn.unizg.hr (A.V.); ivandragicevic007@gmail.com (I.D.)
* Correspondence: zeljko.duic@rgn.unizg.hr

Abstract: Fractured aquifers, especially dolomites, are important hydrocarbon reservoirs and sources of thermal and groundwater in many parts of the world, especially in the Alpine-Dinaric-Carpathian region. The most dominant porosity type is fracture porosity, which acts as the preferential fluid pathway in the subsurface, thus strongly controlling fluid flow. Outcrops provide valuable information for the characterization of fracture networks. Dolomite rock properties and structural and diagenetic processes result in fractured systems that can be considered fractals. The fracture network was analyzed on 14 vertical outcrops in 35 digitized photographs. The values of the fractal dimensions varied slightly by the software and method used, but the trends were consistent, which confirms that all methods are valid. Small values of fractal dimension indicate the dominance of a few small or large fractures, and high values of fractal dimension result from a combination of large numbers of small fractures accompanied by a few large fractures. The mean value of the fractal dimension for analyzed fracture networks was 1.648. The results indicate that the fracture network of the Upper Triassic dolomites can be approximated by fractal distribution and can be considered a natural fractal, and values can be extrapolated to higher and lower scales (1D and 3D).

Keywords: fractal dimension; fracture systems; Triassic dolomites; box-counting; radius mass

Citation: Pavičić, I.; Duić, Ž.; Vrbaški, A.; Dragičević, I. Fractal Characterization of Multiscale Fracture Network Distribution in Dolomites: Outcrop Analogue of Subsurface Reservoirs. *Fractal Fract.* **2023**, *7*, 676. https://doi.org/10.3390/fractalfract7090676

Academic Editors: Mei Yin, Mengxi Zhang and Yi Rui

Received: 2 July 2023
Revised: 22 August 2023
Accepted: 24 August 2023
Published: 7 September 2023

1. Introduction

Discontinuities in rocks occur when the rock has lost cohesion due to brittle deformation [1–5] Fractured dolomites can be significant oil and gas reservoirs or geothermal water and/or groundwater aquifers. In most dolomites, fluid flow is established dominantly through faults and fractures [6–8]. The depositional porosity of these rocks is relatively low, usually less than 5% [8], so fracture systems control the main fluid flow. Natural fractures usually comprise complex patterns and spatial distribution in large-scale intervals, from microns to hundreds of kilometers [9–12]. All rocks, especially dolomites, are fractured at some scale (micro, meso, macro-scale), and discontinuities at all scales affect geomechanical and hydrogeological behavior [5,12–19]. The mechanical properties such as rock mass stability, heterogeneity, anisotropy, conductibility, permeability, connectivity, and displacement deformation are related to the distribution pattern, scale, and abundance of fracture zones and fractures [20,21]. Understanding spatial fracture distribution and space-filling patterns is a challenging task relevant to engineering applications such as underground construction, geothermal systems, petroleum reservoir exploration, unconventional shale gas production, groundwater management, CO_2 storage, radioactive waste disposal, and mining of mineral resources [22–30]. Therefore, knowledge and understanding of the properties of fracture systems greatly benefit the management of exploitation, design, and execution of new drill holes and the understanding of the petrophysical characteristics of rocks [7,31].

Direct observation of the fault and fracture systems is often not possible due to the depths at which the rocks are located when they represent reservoirs of oil and gas, geothermal water, and even groundwater. In the petroleum industry, the only exact input data on fractures is one-dimensional (borehole data), but this is often insufficient to model the three-dimensional (3D) distribution of fractures [32]. Also, borehole data refer mainly to small fractures representing a close area around the borehole [32,33]. Discontinuity distribution and fault displacements (10 and more meters) are available after seismic data interpretation [32,34]. There is a significant gap in knowledge of fault and fracture systems between the borehole and seismic data resolution. The characteristics of the fracture systems in this interval are the most important for characterizing the properties of the reservoirs or aquifers [32]. To precisely model such fractures, a detailed survey of rock outcrops on the surface ("analog outcrop studies") can be of great help [7,35–39]. Rock outcrops are extremely reliable data sources on fracture systems because they contain continuous 2D to 3D data on their geometry and distribution, depending on some controlling factors such as the thickness of layers and the geological structure in which the observed outcrop is located [32,40]. However, three-dimensional porosity data are rarely available, and their acquisition is often very expensive [41]. Two-dimensional (outcrops, quarries, orthophotos, geophysical data, microscopic preparations, etc.) and one-dimensional data (borehole data, "scanlines", etc.) are much more common.

Many geological objects, processes, and phenomena appear in a large interval of scales, from the scale of the crystal lattice to the regional scale (from microns to hundreds of kilometers), so they are scale-independent. This property is called self-similarity; objects, processes, or phenomena characterized by this property are called fractals. Fractal geometry is often applicable to describing geological objects and phenomena that exhibit scale-independent behavior [14]. Fractals and fractal geometry have found great use in various fields of geology, especially when "classical" geometry is not sufficient to describe irregular objects in nature [42,43]. Many researchers have investigated the fractal behaviors of different natural phenomena but also from fractures from outcrop observations and experiments [8,12,14,21,43–62]. In fault/fracture characterization, fractal geometry is used to describe fault/fracture patterns [11,13,21,43,57,63–74], fluid flow through fracture or double porosity media [12,52,56,56,75–78] and discrete fracture networks (DFNs) [21,31,32,79–88].

This research systematically investigated the fractal characterization of fracture system patterns of Upper Triassic dolomites in the Žumberak Mts. in northern Croatia. We digitized 35 outcrop images from 14 outcrops (Figure 1) to measure fractures in multiple scales. The box-counting method of fracture networks is the most popular fractal analysis method [66]. These rocks are regionally the most widespread geological formation in the Alpine–Carpathian–Dinarides region, with huge significance for the industry since they represent a major geothermal aquifer. Furthermore, Upper Triassic dolomites are significant groundwater aquifers and hydrocarbon reservoirs that can be used for crushed stone [89]. Due to intensive fracturing and/or recrystallization of these dolomites on the surface, there are only a few papers dealing with the porosity description and quantification, so this paper presents a significant contribution to the understanding of the porosity distribution and quantification of these rocks.

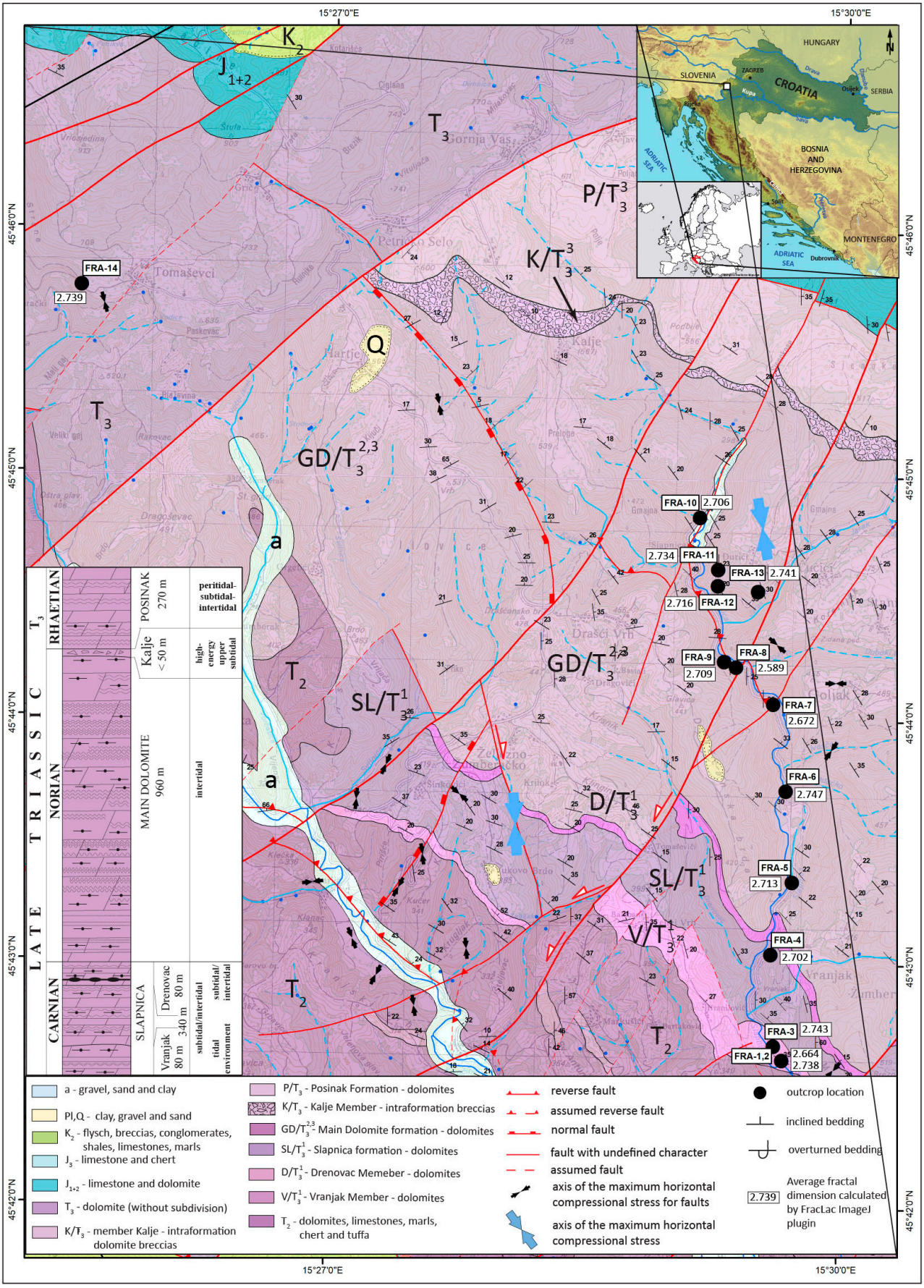

Figure 1. The geological map of the research area with outcrop locations [8,89,90].

2. Geological Setting

Upper Triassic dolomites are one of the most dominant and regionally widespread geological formations in the Alpine–Carpathian–Dinarides region. Most of this Upper Triassic dolomite succession is presented by the Main Dolomite Formation (original name is Hauptdolomite [91]. The most important characteristics of the Upper Triassic dolomites are huge lateral, widespread and large thicknesses from 300 m up to 3000 m [7,89,90,92–96]. These geological settings and significant porosity result in large groundwater and geothermal water aquifer potential.

The research area is located in the Žumberak Mts, in the northwest part of Croatia, where the Upper Triassic dolomites are developed to a total thickness of 1590 m (Figure 1) [89,90]. This area was selected because it is a nearly tectonically undisturbed area required for pore size analysis. Three formations were singled out: Slapnica (with members Vranjak and Drenovac), Main Dolomite (with member Kalje), and Posinak (Figure 1). Within the formations and members, cyclically alternating microfacies were determined: dolomicrite, fenestral dolomite, and stromatolitic dolomite [8,90]. Sedimentary environments have been interpreted as a dynamic shallow-water system from subtidal to shallow intertidal [90]. Tectonic settings are relatively simple, with few major faults, but rocks are not very tectonically disturbed (Figure 1). Layer inclination varies from horizontal up to 57° in the vicinity of the faults. Most of the area is tectonically not disturbed, which was one of the main reasons for having preserved outcrops for fracture pattern analysis.

3. Theoretical Background

The concept of dimension in mathematics can be approached from different points of view, and there are different definitions of dimension [97]. Euclidean and topological dimensions are finite and integer (1,2,3) and roughly define space. Many objects and phenomena in nature can be described with 0, 1, 2, or 3 dimensions (Figure 2A). However, Mandelbrot (1983) [98] noticed that many irregular objects and phenomena appear in nature that cannot be completely defined by topological dimensions. Examples are clouds that are not spheres, flashes of lightning that are not straight lines, mountain belts that are not cones, etc. [98]. Their dimension is described by the Hausdorff (some authors also call it Hausdorff–Besicovich) dimension, which measures how much an object fills a metric space. To understand fractals and fractal dimensions, it is necessary to define concepts such as Hausdorff measure and dimension [99]:

The δ-cover of a set F is a countable or finite union of sets $\{U_i\}$ with radii, $0 < |U_i| \leq \delta$ that cover the set F. Let $F \subset R^n$ and let $s \in [0, \infty)$, for each $\delta > 0$, we define:

$$H^s_\delta(F) = inf\{\sum_{i=1}^{\infty} |U_i|^s : \{U_i\}\} \text{ is a } \delta - \text{cover of } F \quad (1)$$

Therefore, the quantity $H^s_\delta(F)$ presents the minimal sum of the s-th powers of the diameters over all covers of F by sets of diameters not greater than δ.

As δ decreases, the set of permissible covers of F (in Equation (1)) is reduced [99], and hence, the value of the infimum $H^s_\delta(F)$ does not decrease and approaches the limit value as δ tends to zero [99] (Equation (2)):

$$H^s(F) = \lim_{\delta \to 0} H^s_\delta(F) \quad (2)$$

This limit exists for every subset F of the set R^n, although the limit value is often 0 or ∞. $H^s(F)$ is called the s-dimensional Hausdorff measure of a set F. The Hausdorff measure is a measure that assigns some value from the interval $[0, \infty]$ to each set in R^n. A 0-dimensional Hausdorff measure of a set is the number of points in this set (if the set is finite) and ∞ if the set is infinite. The one-dimensional measure of a smooth curve or line in R^n is equal to the length of that curve. This means the Hausdorff measure generalizes count, length, area, and volume but does not necessarily have to attain positive integer values [99]. According to Equation (1), for an arbitrary set $F \subset R^n$ and if $\delta < 1$, $H^s_\delta(F)$ does

not increase with increasing s, and according to Equation (2), $H^s(F)$ will not increase either. Moreover, if $t > s$ and $\{U_i\}$ is a δ-cover of the set F, then it holds:

$$\sum_i |U_i|^t \leq \sum_i |U_i|^{t-s} |U_i|^s \leq \delta^{t-s} \sum_i |U_i|^s \tag{3}$$

Calculating the infimum over all δ-coverings in Equation (3) results in Equation (4):

$$H_\delta^t(F) \leq \delta^{t-s} H_\delta^s(F) \tag{4}$$

By letting $\delta \to 0$ in Equation (4), it follows that if $H^s(F) < \infty$, then $H^t(F) = 0$ for every $t > s$. The graph shows that there is a critical value of s at which $H^s(F)$ "jumps" from ∞ to 0 (Figure 2B).

This critical value is called the Hausdorff dimension of the set F, denoted $dim_H F$, and is defined for each set $F \subset R^n$:

$$dim_H F = D = inf\{s \geq 0 : H^s(F) = 0\} = sup\{s : H^s(F) = \infty\} \tag{5}$$

If the upper limit (supremum) of the empty set is stated value 0, then:

$$H^s(F) = \begin{cases} \infty \; if \; 0 \leq s < dim_H F \\ 0 \; if \; s > dim_H F \end{cases} \tag{6}$$

If $s = dim_H F$, then $H^s(F)$ can be 0, ∞, or it can satisfy:

$$0 < H^s(F) < \infty \tag{7}$$

The Hausdorff dimension is often used to describe the fractal dimension (F_{dim}) of complex objects in nature. A point has Hausdorff dimension D = 0, a line D = 1, a surface D = 2, and a cube D = 3 (Figure 2A). Mandelbrot defined a fractal as a set, an object, or a phenomenon whose Hausdorff dimension (D) is greater than the topological one, where the dimension D is defined by [58,98]:

$$N_i = \frac{C}{r_i^D} \tag{8}$$

where:

N_i—number of objects or fragments characterized by linear dimension r_i; C—proportionality constant; D—fractal (Hausdorff dimension) dimension that is calculated by (from Equation (8)):

$$D = \frac{\ln\left(\frac{N_{i+1}}{N_i}\right)}{\ln\left(\frac{r_i}{r_{i+1}}\right)} = \frac{\log\left(\frac{N_{i+1}}{N_i}\right)}{\log\left(\frac{r_i}{r_{i+1}}\right)} \tag{9}$$

where: *ln* is logarithm with base e, and log is logarithm with base 10.

Natural (statistical) fractals have the following properties [61]:

(1) The parts of the object have the same structure as the object as a whole, except that they are slightly deformed in different scales (there are small fluctuations in the degree of fractality between scales)—a property of self-similarity.
(2) Forms are often irregular and fragmented and remain so in all scales in which they exist.
(3) They are created through an iterative process.
(4) They have a fractal dimension.

The basic property of fractal distribution is scale independence. Mathematically, Equation (8) can be applied to an infinitely large-scale interval. However, natural fractals appear on a scale limited by lower and upper limits, which also applies to fractal distributions [100]. Fragmentation should be considered to understand how to apply the

fractal distribution to real data sets. Fragmentation is crucial to many geological processes and phenomena [61]. Rocks can be fragmented in various ways—by tectonic processes that include faulting, the formation of fissures, and fracture systems through which the rock can be further fragmented by tectonic processes or weathering [61,100]. The formation of fractures is a non-linear process, so even the simplest distribution of fractures and fracture systems is demanding and challenging to model. Fractal geometry allows quantifying geometric shapes that repeat over a certain range of scales [66]. The fragmentation process (Figure 3A) and an example photograph of an Upper Triassic dolomite sample (Figure 3B) indicate that fractal geometry can quantify the scale range of the spatial distribution of fracture systems in dolomites. Also, the fractal description of fracture systems can represent a basis for analyzing fluid flow through rocks because the fluid flow that occurs through a fractal medium should also have fractal properties [43,59,66].

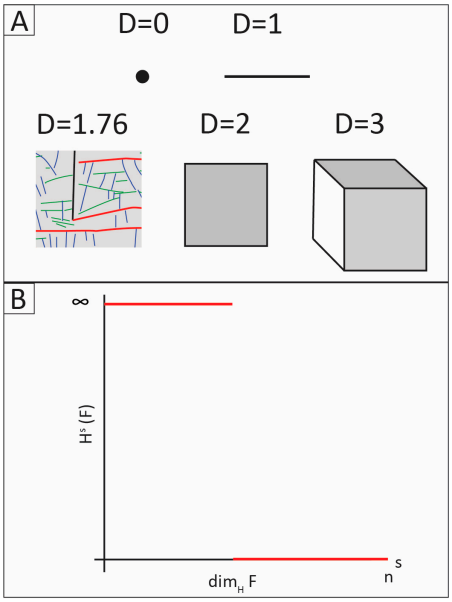

Figure 2. (**A**) Fractal dimensions of Euclidean objects (point, line, area, and body with D = 0, 1, 2, and 3) and an example of a fractal fracture network with a fractal dimension of D = 1.76. (**B**) A graph showing the dependence of the Hausdorff measure ($H^s(F)$) on the parameter s. The Hausdorff dimension is the value of s at which s falls from ∞ to 0 [99].

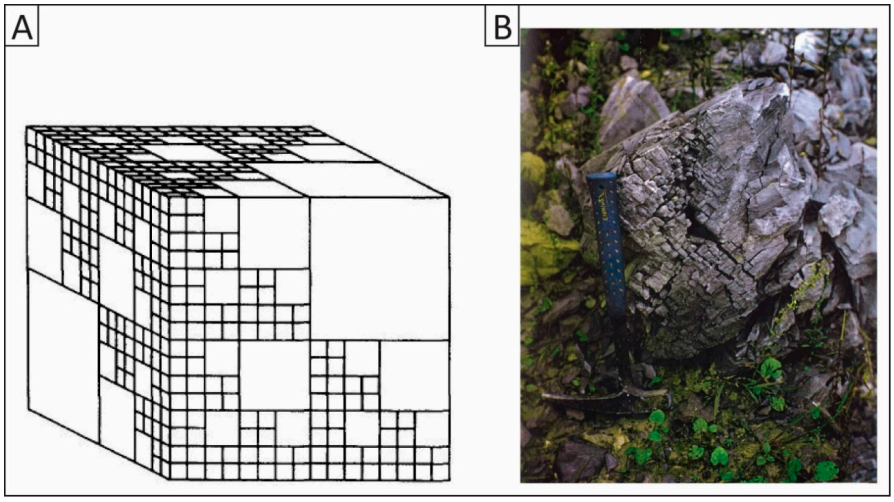

Figure 3. (**A**) Theoretical model (three-dimensional fractal model of fragmentation) according to [101] and (**B**) fracture porosity in the Late Triassic dolomites in Žumberak Mts.

4. Materials and Methods

The F_{dim} of fracture patterns can be estimated from photographs of outcrops and samples (Figure 4) [43,52,100,102–104]. Image processing of the outcrop photographs can be a powerful tool for data acquisition, preparation, and analysis of fracture systems in rocks [103]. As the photographs are characterized by two dimensions (length and width), the F_{dim} of the fracture systems in the photographs is $1 < D < 2$. The applicability of F_{dim} in defining porosity features is that it theoretically allows the extrapolation of the estimated dimensions to a higher order (from 1D to 2D, or from 2D to 3D) [14,43,98,100,104] by a simple relationship:

$$D_{2-D} = D_{1-D} + 1 \quad (10)$$

$$D_{3-D} = D_{2-D} + 1 \quad (11)$$

whereby: D_{3-D} = fractal dimension of the object observed in 3D space; D_{2-D} = fractal dimension of the object observed in 2D space; D_{1-D} = fractal dimension of the object observed in 1D space.

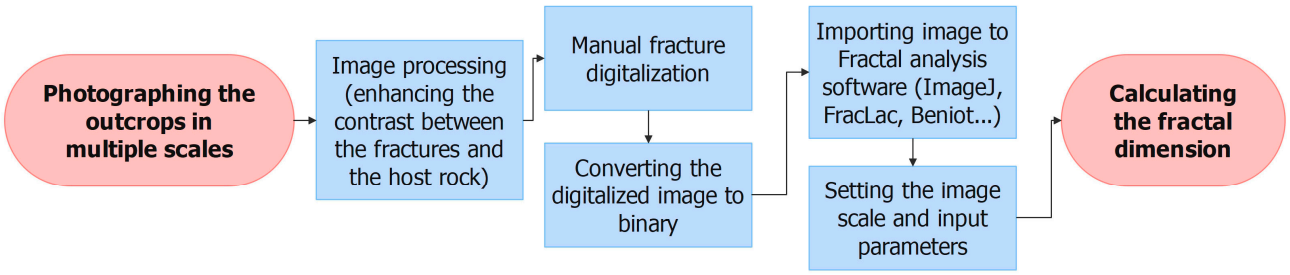

Figure 4. Outcrop image processing and fractal dimension calculation flowchart.

Equations (10) and (11) are valid because the intersection of a 3D fractal with a plane will result in a 2D fractal with the fractal dimension $D = D_{3-D} - 1$. Both equations are valid only for isotropic and deterministic fractals [105]. For real objects, in our case, dolomite rocks, the more applicable relation is [43]:

$$D_{2-D} = D_{1-D} + 1.06 \quad (12)$$

Fractal analysis using computer programs is most often performed with the Box-counting and radius mass methods. In the box-counting method, the photograph of the outcrop is covered with a square grid of different square dimensions. For each value of square size, the cells containing the pixels covering the object in the photo are counted. The F_{dim} is then calculated by Equation (9). The computer program iteratively covers the given image with squares of different dimensions. The relationship between the size of the square and the number of squares that cover the object results in a log–log line whose slope represents the F_{dim} of the object. The second most used method is the "Radius mass" method. With the "Radius mass" method, the algorithm arbitrarily determines specific points and draws circles of different radii that grow iteratively around them. The ratio of black (observed object) and white pixels (background) is counted at each iteration. Each step counts the total number of occupied pixels inside the circle. The paper used both methods for F_{dim} calculation to compare results.

For the research, 14 outcrops in the Upper Triassic dolomites were photographed in detail, and 35 photographs were selected for further analysis (Figure 1, Table 1, Supplementary File S1). Numerous automatic algorithms were tested to digitize the fractures in the photographs. Still, the results were unsatisfactory due to large noise (fracture aperture and infill, vegetation, crushed rock fragments etc.) in the photographs, so software could not delineate fractures from the host rock. In other words, it was not possible to satisfactorily delineate fractures from the rock by automatic algorithms. Thus, all photographs were digitized manually (Figures 4 and 5). Photographs were

adjusted in color, brightness, and hue to more easily distinguish fractures from the rock (Figure 5A). The outcrop was then delineated from the surrounding vegetation, and the region of interest (ROI) was defined. Fractures were then manually traced in the Adobe Illustrator 2021 software (Figure 5B).

Table 1. Placemarks, photograph names (photographs are presented in Supplementary File S1), and basic geological information.

Placemark	Photograph Name	X (HTRS)	Y (HTRS)	Formation (Member)	Age	Vegetation in Image
FRA-1	IMG_1571	421,714.6204	5063852.169	Slapnica (Vranjak)	Carnian	YES
FRA-2	IMG_1683	421,714.6204	5,063,852.169	Slapnica (Vranjak)	Norian-Rhaetian	YES
	IMG_1705					NO
	IMG_1710					NO
	IMG_1712					NO
FRA-3	IMG_1766	421,650.0122	5,065,208.69	Slapnica (Vranjak)	Carnian	YES
	IMG_1769					NO
	IMG_1774					NO
	IMG_1779					NO
FRA-4	IMG_1796	421,632.2322	5,064,660.356	Main Dolomite	Norian-Rhaetian	YES
FRA-5	PAN_24	421,794.3962	5,065,208.69	Main Dolomite	Norian-Rhaetian	YES
	PAN_24_B					YES
	IMG_1870					YES
	IMG_1887					NO
	IMG_1887 (O)					NO
FRA-6	PAN_1904-1911	421,689.2998	5,064,905.212	Main Dolomite	Norian-Rhaetian	YES
FRA-7	PAN_1935-1952	421,653.4046	5,066,561.463	Main Dolomite	Norian-Rhaetian	YES
	IMG_1964					NO
FRA-8	IMG_2012	421,372.0408	5,066,843.261	Main Dolomite	Norian-Rhaetian	YES
	IMG_2016					NO
	IMG_2020					NO
FRA-9	PAN-51	421,280.3314	5,066,884.165	Main Dolomite	Norian-Rhaetian	YES
	IMG_2032 (O)					YES
FRA-10	PAN_2056-2060	421,099.8951	5,067,986.247	Main Dolomite	Norian-Rhaetian	YES
	PAN_2062-2075					YES
	IMG_2088					YES
	IMG_2091					NO
FRA-11	IMG_2106	421,235.9503	5,067,584.525	Main Dolomite	Norian-Rhaetian	NO
FRA-12	IMG_2110	421,232.7753	5,067,460.7	Main Dolomite	Norian-Rhaetian	YES
	IMG_2117					NO
	IMG_2121					YES
	IMG_2119					NO
FRA-13	PAN_2188-2191	421,539.1634	5,067,416.25	Main Dolomite	Norian-Rhaetian	YES
FRA-14	PAN_1647-1653	416,393.1683	5,069,792.002	Main Dolomite	Norian-Rhaetian	YES
	IMG_1656					NO

After all fractures were digitized, images were converted from color photographs into binary photographs (black and white) by ImageJ 1.53.c software to estimate the fractal dimensions of the fracture patterns (Figure 5C). The purpose of the procedure was to obtain binary photos that optimally showed the fractures in the rock, so that the software

operated only with white and black pixels. Processing is the most demanding process of photo preparation for fractal analysis. It includes all actions by which the image is prepared for conversion into the binary form: removal of vegetation, manual digitization of fractures, and conversion of the photograph into binary (Figure 5A–C). Binary photographs consisted only of black and white pixels; in our case, black represented fractures, and white represented rock (Figure 5C).

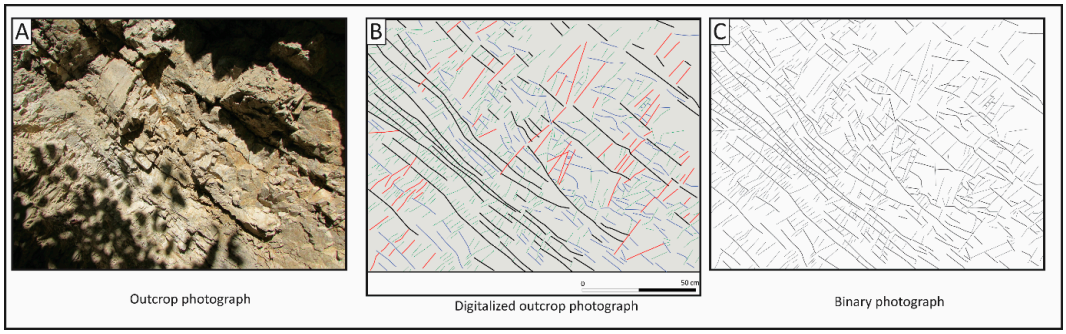

Figure 5. (**A**) photograph of the outcrop; (**B**) digitized photo of the outcrop; (**C**) binary photograph (FRA-2, photo IMG_1705).

In binary photos, if the fractures are represented by a value of 1, the rock is represented by 0. The vegetation is also represented by a value of 0, which reduces the F_{dim} of the fracture pattern in the photograph. To overcome the vegetation problem, it was necessary to create boundaries within the binary photo region of interest (ROI) within which the F_{dim} was evaluated (Figure 6). When the ROI was defined, the program calculated the F_{dim} only within the ROI, eliminating vegetation's influence on the calculation.

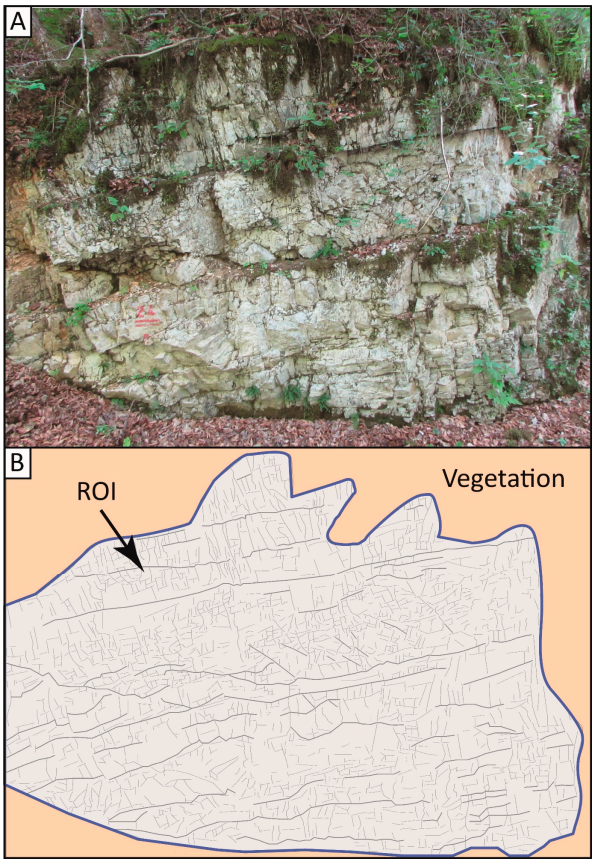

Figure 6. (**A**) Photograph of the outcrop with vegetation (FRA-9, IMG_PAN-51), (**B**) Example of ROI determination where vegetation occupies a significant area in the photograph.

Several programs with several algorithms were used to compare the results and evaluate which program and algorithm gave the most reliable results. To estimate the F_{dim} of the fracture systems, ImageJ 1.53c®, FracLac (supplement for ImageJ) [106], and Fractalyse 2.4. ® http://www.fractalyse.org, accessed 20 April 2021) were used (Supplementary File S2). Of the programs used, only FracLac could make an irregular ROI. An ROI could also be made using Fractalyse, but only in a square shape, which is often unsatisfactory (Figure 6).

For every outcrop photo, we calculated 2D porosity as the ratio between white and black pixels in ImageJ software.

5. Results

The calculated fractal dimensions differed between the software and methods used. Overall, the F_{dim} of the fracture complex of the Upper Triassic dolomites of Žumberak ranged from 1.465 to 1.802 (Figure 7, Supplementary File S3). The Fractalyse software obtained the lowest and highest values. The Fractalyse box-counting method obtained the lowest values and the highest by the Fractalyse radius mass method. Results of FracLac box-counting analysis were usually in between the results from Fractalyse software.

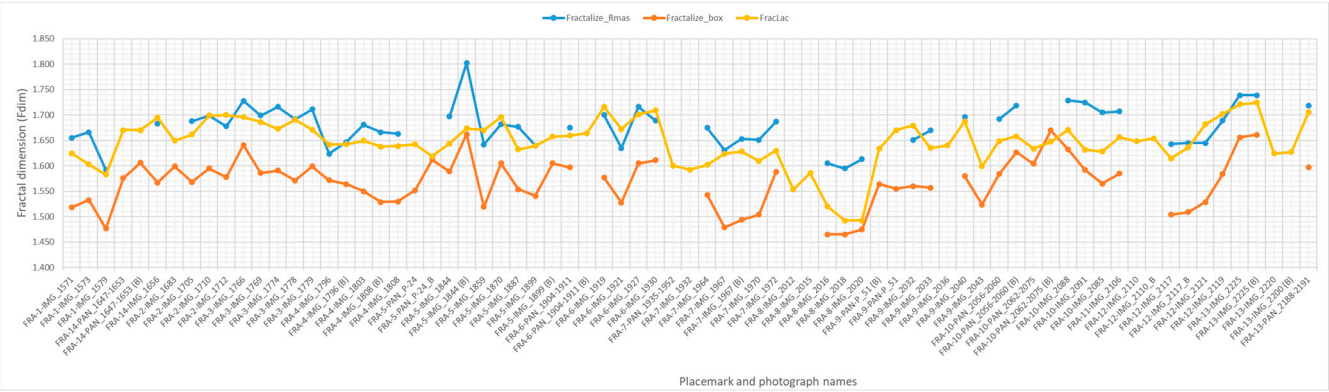

Figure 7. Fractal dimensions were obtained by Fractalyse box counting, Fractalyse radius mass, and FracLac box-counting analysis on outcrop photographs.

The main reason for the relatively low values obtained by Fractalyse was that it was impossible to select the ROI, so the fracture systems in the photographs with vegetation had underestimated F_{dim} values (or we did not calculate F_{dim} at all). In Fractalyse, it is possible to create only a square-shaped ROI, which for most photos was not enough to exclude areas with vegetation from the calculation. The F_{dim} mainly depends on the number of iterations the program performs and the sizes of the squares with which the image is covered at each iterative step. So, we performed multiple calculations until the results of F_{dim} did not change regarding box sizes and the number of iterations. Notably, the F_{dim} trends obtained with all programs were largely consistent (Figure 7, Supplementary File S3). This confirmed that all methods are valid and that fracture systems control the values of F_{dim} (Figure 7, Supplementary File S3).

Fractalyse box-counting analysis resulted in an F_{dim} ranging from 1.465 to 1.670, with an average of 1.568 and a median of 1.572. Photographs with large vegetation areas were not analyzed. Fractalyse radius-mass analysis resulted in an F_{dim} ranging from 1.592 to 1.802, with an average of 1.678 and a median of 1.682. Again, photographs with large vegetation areas were not analyzed.

FracLac analysis was conducted only with the box-counting method, and the results were usually between the results obtained by Fractalyse. FracLac fractal dimensions for Upper Triassic dolomites ranged from 1.492 to 1.725, with an average of 1.646 and a median of 1.649 (Supplementary File S3). Even though there were differences between the algorithms and software used, the differences were very consistent in all analyzed images, indicating that differences resulted from different calculation parameters (Figure 8).

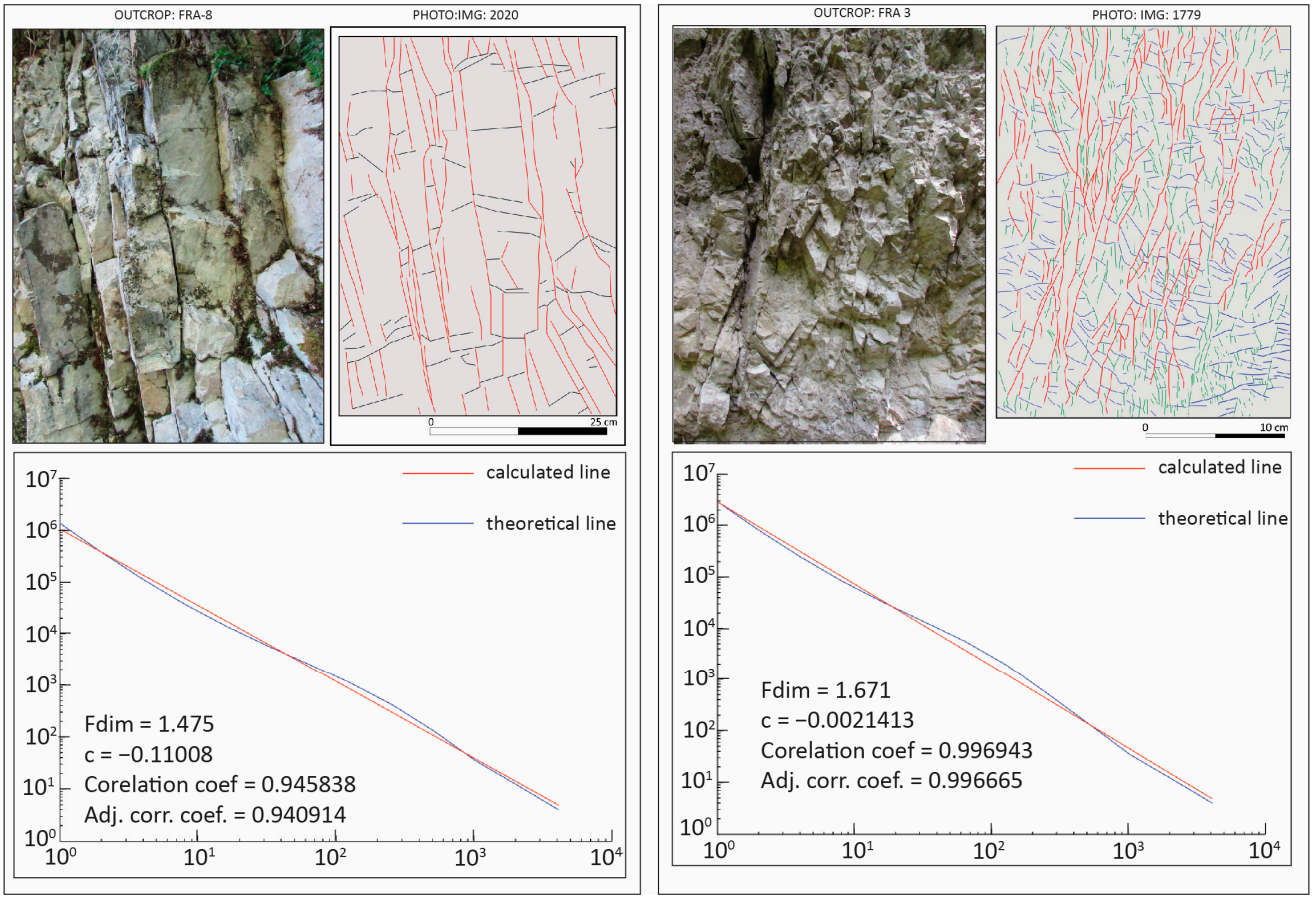

Figure 8. Comparison of fracture network with low fractal dimension (**A**) and high fractal dimension (**B**).

Generally, the lowest values were related to fracture patterns of lower complexity, and higher values corresponded to higher complexity (Figure 8). Small values of F_{dim} indicated the dominance of a small number of large fractures or small number of small fractures (Figure 8A). Many smaller fractures, together with a small number of large ones, contributed to the complexity of the fracture system and, by that, to a higher value of F_{dim} (Figure 8B). The values for fractal dimensions obtained with all software and algorithms can be divided into three groups concerning the fracture system architecture:

(1) Small F_{dim} values (Fractalyse$_{box\text{-}count}$: from 1.465 to 1.525; Fractalyse$_{rmass}$: from 1.592 to 1.650; and FracLac: from 1.492 to 1.600). Small values of fractal dimensions were obtained for outcrops with a relatively small number of fractures, i.e., less fragmented outcrops, or where large fractures dominated (Figure 8A). These were outcrops where not all sets of fractures had been developed or were not visible. In these parts of the outcrop, the fracture system's complexity was lower, resulting in lower F_{dim} values.

(2) Average F_{dim} values (Fractalyse$_{box\text{-}count}$: from 1.525 to 1.625; Fractalyse$_{rmass}$: from 1.650 to 1.700; and FracLac: from 1.600 to 1.675). Most of the analyzed photos of outcrops belonged in this interval. This interval could be considered representative of the Upper Triassic dolomites of Žumberak.

(3) Large F_{dim} values (Fractalyse$_{box\text{-}count}$: from 1.625 to 1.670; Fractalyse$_{rmass}$: from 1.700 to 1.802; and FracLac: from 1.675 to 1.725). The largest fractal dimensions were obtained for the more fractured parts of the outcrops, which resulted in a more complex fracture system (Figure 8B). Fractures filled large portions of the analyzed space irregularly, so the fracture network's complexity was high, resulting in high fractal dimension values.

Two-dimensional porosity (P_{22}) was calculated for 35 outcrop photographs and ranged from 2.84% up to 8.99%, with an average value of 5.7% (Figure 9). Since porosity is a three-dimensional rock property, these values should be checked by some 3D method in the future to see how representative they are of the rock mass. The fractures were digitized as lines, and the aperture of the fractures was not considered, which could affect the porosity values. A correlation diagram between 2D porosity and F_{dim} was prepared to analyze the dependence between these two parameters (Figure 10). There was no visible correlation between the two parameters, which indicated that more or less complex fracture systems can result in higher and lower porosities. Furthermore, for better fracture network description in 2D, it was necessary to analyze both parameters.

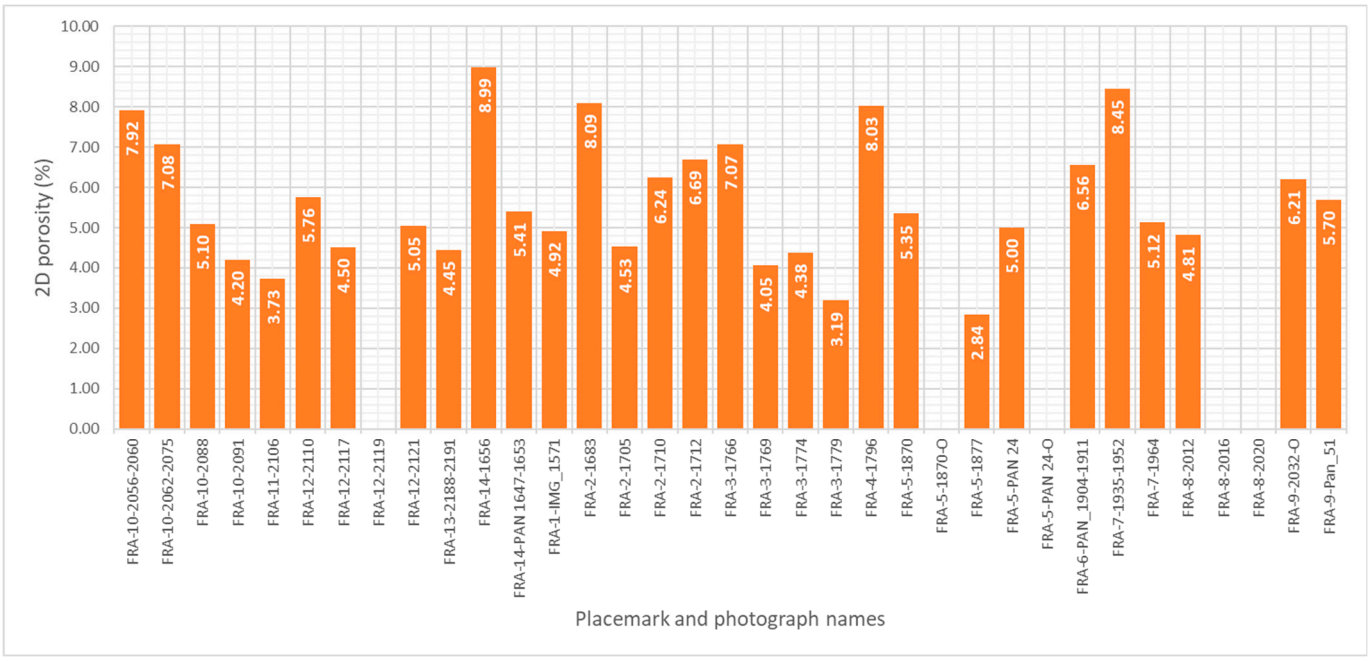

Figure 9. Two-dimensional porosity of the Upper Triassic dolomites obtained from outcrop photographs.

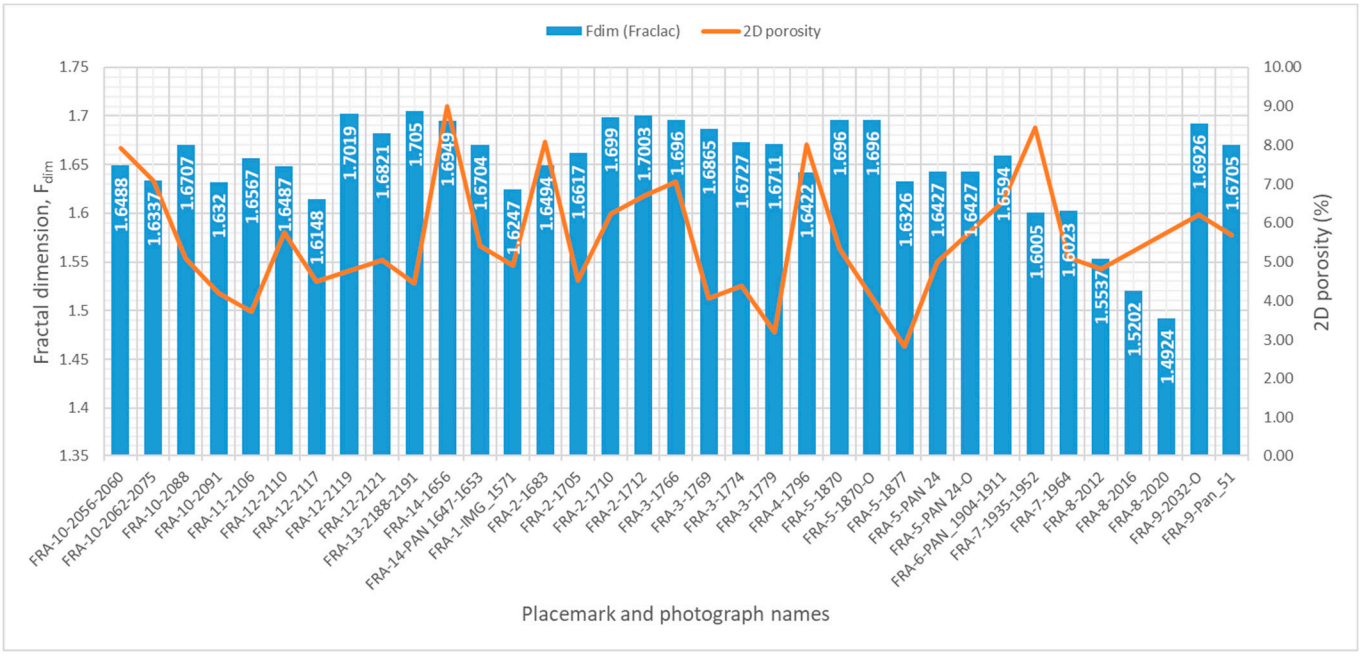

Figure 10. Relation of 2D porosity and fractal dimension of fracture networks in the outcrop photographs.

The fractal dimension of fracture systems is a measure of the complexity of the fracture system. It depends on the rock type and the tectonic history of the investigated area [43]. Two-dimensional (2D) fractal dimensions close to 1 indicate a small number of fractures, i.e., a simple fracture architecture. Large values, close to 2, indicate an extremely complex fracture system: the rock is extremely fractured or fragmented by a complex network of fractures [101]. The calculated values for the fracture systems in the photographs and the mean values of individual outcrops were mostly greater than 1.585 (Figures 7–10).

The mean value of F_{dim} for all outcrops was 1.646. Dolomites are among the most fractured rocks in nature [6,43,107], and large values of the fractal dimension of fracture systems are expected of them. As the fractal dimension measures complexity, different fracture systems of different geometries but the same complexity will result in the same value of fractal dimension. The results indicated that the fracture system of the Upper Triassic dolomites could be approximated by fractal distribution and considered a natural fractal. Because of this, the spatial and statistical geometric properties of the fracture systems could be extrapolated to higher and lower scales by Equation (12).

The extrapolation of the fractal dimension from 2D to 3D by Equation (12) [43] resulted in F_{dim} values for Upper Triassic dolomites, ranging from 2.53 to 2.86 (Table 2) depending on the software and the algorithm. Average values were between 2.62 (Fractalyse box counting) and 2.74 (Fractalyse Radius Mass) (Table 2). Generally, the results of this research were very consistent with results from [43], who analyzed similar rocks with similar methodology in Slovenia.

Table 2. Average, median, maximum, and minimum Fdim were calculated for individual images and averaged for outcrops. F_{dim} ext is F_{dim} extrapolated from 2D to 3D by Equation (12).

	Fractalyse (Radius Mass)				Fractalyse Box Counting				FracLac (Plugin for ImageJ)			
	F_{dim}	AVG (per Outcrop)	F_{dim} ext	AVG ext (per Outcrop)	F_{dim}	AVG (per Outcrop)	F_{dim} ext	AVG ext (per Outcrop)	F_{dim}	AVG (per Outcrop)	F_{dim} ext	AVG ext (per Outcrop)
AVG	1.68	1.68	2.74	2.74	1.57	1.56	2.63	2.62	1.65	1.65	2.71	2.71
MEDIAN	1.68	1.68	2.74	2.74	1.57	1.58	2.63	2.64	1.65	1.65	2.71	2.71
MAX	1.80	1.73	2.86	2.79	1.67	1.64	2.73	2.70	1.72	1.69	2.78	2.75
MIN	1.59	1.60	2.65	2.66	1.47	1.47	2.53	2.53	1.49	1.53	2.55	2.59

6. Discussion and Conclusions

The fractal dimension is a measure of the complexity of the analyzed pattern. Different fracture systems of different geometry but of the same complexity will result in the same fractal dimension. In this paper, we used manual fracture extraction from photographs. There are many semi-automatic or automatic algorithms published in the literature. Still, after trying a few of them, the results were not satisfactory due to several issues: (i) dolomites are highly fractured by fractures of multiple orders (from larger to smaller); (ii) fractures sometimes had an aperture that was filled with crushed dolomite or clay that was problematic for the algorithms to overcome; (iii) due to high fracturing, there were pieces of rock on the outcrop that were often considered as fracture traces, so the postprocessing of the results could take a long time. Considering everything, we found that only manual digitization (that could be biased) applied to this type of rock.

We analyzed the impact of fracture patterns in outcrop images on their fractal dimensions. The results can be summarized as follows:

Fractal dimensions of fracture systems in outcrops can be subdivided into three categories:

(1) Small 2D F_{dim} values ($Fractalyse_{box\text{-}count}$: from 1.465 to 1.525; $Fractalyse_{rmass}$: from 1.592 to 1.650; and FracLac: from 1.492 to 1.600).
(2) Average 2D F_{dim} values ($Fractalyse_{box\text{-}count}$: from 1.525 to 1.625; $Fractalyse_{rmass}$: from 1.650 to 1.700; and FracLac: from 1.600 to 1.675). Most of the analyzed photos of outcrops were in this category.
(3) Large 2D F_{dim} values ($Fractalyse_{box\text{-}count}$: from 1,625 to 1.670; $Fractalyse_{rmass}$: from 1.700 to 1.802; and FracLac: from 1.675 to 1.725).

Simple Equation (12) could extrapolate from 2D F_{dim} to 3D, and the results for the analyzed outcrops ranged from 2.53 to 2.86, with average values between 2.62 ($Fractalyse_{box\text{-}count}$) and 2.74 ($Fractalyse_{Rmass}$) (Table 2).

2D Porosity (P_{22}) for Upper Triassic dolomites was in the interval from 2.84% up to 8.99%, with an average value of 5.7%.

Dolomites are among the most highly fractured rocks [6,43,107], and high values of the fractal dimension of fracture systems are expected. As the fractal dimension is a measure of complexity, different fracture systems with different geometries but of the same complexity will result in the same fractal dimension. That is why the spatial and statistical geometric properties of the fractal fracture network can be extrapolated to higher and lower scales. Verbovšek, 2009 [43,108] analyzed the fractal dimensions of fracture systems on the Middle and Upper Triassic dolomites of Slovenia using different measurement methods. The values of the fractal dimensions for the "box-flex" and "box-rotate" methods were 1.78±0.02. The results of the "Box-counting-Full Method", which are comparable to the results in this research, were in the interval from 1.47 to 1.59 [43], which is, on average, somewhat lower than the results of this research. The porosity of the T_3 dolomite of the Sella Group (Dolomites, northern Italy) [7] can be compared with the results of this study. The fracture porosity of the Main Dolomites formation of the Sella group reached 2.4%. Such a "small" value of fracture porosity can be attributed to only two sets of fractures in the analyzed area [7]. Published dolomite porosity values range from 1 to 27%, where porosity is not divided into fracture, sedimentary and diagenetic [6,7]. This study makes a significant contribution to the analysis of fracture networks of dolomites (especially Upper Triassic dolomites) since there are only a few papers dealing with the subject due to excessive fragmentation and fracturing of dolomites, which make analysis almost impossible.

In carbonate reservoirs, the permeability is usually influenced by the fracture network [63]. Depending on the fracture network characteristics, fractures can behave as fluid flow conduits, barriers, and combined conduit–barriers [63,109–111]. Detailed fracture description and parameter quantification then become crucial to analyze and predict the fluid flow behavior in subsurface aquifers or reservoirs [63,112,113]. The results indicate that the fracture system of the Upper Triassic dolomites can be approximated by fractal distribution and can be considered a natural fractal. Because of this, the fracture system's spatial and statistical geometric properties can be extrapolated to higher and lower scales. Natural fracture networks in the subsurface are three-dimensional phenomena. With current technology, such as outcrop mapping, borehole logging, and 3D seismic surveys, performing a 3D fracture network survey is almost impossible. Therefore, investigating fractal characteristics of 3D fracture networks is challenging but very useful for fracture characterization and can be great input for DFN models that are used for 3D fluid flow modeling.

Supplementary Materials: The following supporting information can be downloaded at: https://www.mdpi.com/article/10.3390/fractalfract7090676/s1, Supplementary File S1—outcrop photographs and digitized images of the outcrops. Supplementary File S2—Fractal dimension charts for each image calculated by Fractalyse. Supplementary File S3—Table with all calculated parameters for all images and outcrops.

Author Contributions: Conceptualization, I.P.; methodology, I.P. and A.V.; software, I.P., Ž.D. and A.V.; validation, I.P., Ž.D., A.V. and I.D.; formal analysis, I.P. and A.V.; investigation, I.P., Ž.D., A.V. and I.D.; resources, I.P. and Ž.D.; data curation, I.P. and A.V.; writing—original draft preparation, I.P.; writing—review and editing, I.P., A.V., I.D. and Ž.D.; visualization, I.P. and A.V.; supervision, Ž.D. and I.D.; project administration, I.P.; funding acquisition, I.P. and Ž.D. All authors have read and agreed to the published version of the manuscript.

Funding: This research received no external funding.

Data Availability Statement: Data are available on request due to privacy restrictions. Data presented in this study are available on request from the first author, Ivica Pavičić (ivica.pavicic@rgn.unizg.hr).

Conflicts of Interest: The authors declare no conflict of interest. The funders had no role in the design of the study; in the collection, analyses, or interpretation of data; in the writing of the manuscript, or in the decision to publish the results.

References

1. Price, N.J. *Fault and Joint Development in Brittle and Semibrittle Rock*; Pergamon Press: Oxford, UK, 1966.
2. Ramsay, J.G. *Folding and Fracturing of Rocks*; McGraw-Hill: New York, NY, USA, 1967; ISBN 1-930665-89-X.
3. Hancock, P.L. Brittle Microtectonics: Principles and Practice. *J. Struct. Geol.* **1985**, *7*, 437–457. [CrossRef]
4. Ramsay, J.G.; Huber, M.I. The Techniques of Modern Structural Geology. Volume 2: Folds and Fractures. *Geol. Mag.* **1988**, *125*, 316–317.
5. McGinnis, R.N.; Ferrill, D.A.; Morris, A.P.; Smart, K.J.; Lehrmann, D. Mechanical Stratigraphic Controls on Natural Fracture Spacing and Penetration. *J. Struct. Geol.* **2017**, *95*, 160–170. [CrossRef]
6. Aguilera, R. *Naturally Fractured Reservoirs*; PennWell Books: Tulsa, OK, USA, 1995; 521p.
7. Antonellini, M.; Mollema, P.N. A Natural Analog for a Fractured and Faulted Reservoir in Dolomite: Triassic Sella Group, Northern Italy. *Am. Assoc. Pet. Geol. Bull.* **2000**, *84*, 314–344. [CrossRef]
8. Pavičić, I.; Briševac, Z.; Vrbaški, A.; Grgasović, T.; Duić, Ž.; Šijak, D.; Dragičević, I. Geometric and Fractal Characterization of Pore Systems in the Upper Triassic Dolomites Based on Image Processing Techniques (Example from Žumberak Mts, NW Croatia). *Sustainability* **2021**, *13*, 7668. [CrossRef]
9. Anders, M.H.; Laubach, S.E.; Scholz, C.H. Microfractures: A Review. *J. Struct. Geol.* **2014**, *69*, 377–394. [CrossRef]
10. Zoback, M.D.; Gorelick, S.M. Earthquake Triggering and Large-Scale Geologic Storage of Carbon Dioxide. *Proc. Natl. Acad. Sci. USA* **2012**, *109*, 10164–10168. [CrossRef] [PubMed]
11. Gutierrez, M.; Youn, D.-J. Effects of Fracture Distribution and Length Scale on the Equivalent Continuum Elastic Compliance of Fractured Rock Masses. *J. Rock Mech. Geotech. Eng.* **2015**, *7*, 626–637. [CrossRef]
12. Zhu, W.; Lei, G.; He, X.; Patzek, T.W.; Wang, M. Fractal and Multifractal Characterization of Stochastic Fracture Networks and Real Outcrops. *J. Struct. Geol.* **2022**, *155*, 104508. [CrossRef]
13. Watanabe, K.; Takahashi, H. Fractal Geometry Characterization of Geothermal Reservoir Fracture Networks. *J. Geophys. Res. Solid Earth* **1995**, *100*, 521–528. [CrossRef]
14. Bonnet, E.; Bour, O.; Odling, N.E.; Davy, P.; Main, I.; Cowie, P.; Berkowitz, B. Scaling of Fracture Systems in Geological Media. *Rev. Geophys.* **2001**, *39*, 347–383. [CrossRef]
15. Berkowitz, B. Characterizing Flow and Transport in Fractured Geological Media: A Review. *Adv. Water Resour.* **2002**, *25*, 861–884. [CrossRef]
16. Fountain, A.G.; Jacobel, R.W.; Schlichting, R.; Jansson, P. Fractures as the Main Pathways of Water Flow in Temperate Glaciers. *Nature* **2005**, *433*, 618–621. [CrossRef] [PubMed]
17. Follin, S.; Hartley, L.; Rhén, I.; Jackson, P.; Joyce, S.; Roberts, D.; Swift, B. A Methodology to Constrain the Parameters of a Hydrogeological Discrete Fracture Network Model for Sparsely Fractured Crystalline Rock, Exemplified by Data from the Proposed High-Level Nuclear Waste Repository Site at Forsmark, Sweden. *Hydrogeol. J.* **2014**, *22*, 313–331. [CrossRef]
18. He, X.; Hoteit, H.; Al Sinan, M.M.; Kwak, H.T. Modeling Hydraulic Response of Rock Fractures under Effective Normal Stress. In Proceedings of the ARMA/DGS/SEG International Geomechanics Symposium, Virtual, 3–5 November 2020.
19. He, X.; Sinan, M.; Kwak, H.; Hoteit, H. A Corrected Cubic Law for Single-Phase Laminar Flow through Rough-Walled Fractures. *Adv. Water Resour.* **2021**, *154*, 103984. [CrossRef]
20. Odling, N.E. Scaling and Connectivity of Joint Systems in Sandstones from Western Norway. *J. Struct. Geol.* **1997**, *19*, 1257–1271. [CrossRef]
21. Yangsheng, Z.; Zengchao, F.; Dong, Y.; Weiguo, L.; Zijun, F. Three-Dimensional Fractal Distribution of the Number of Rock-Mass Fracture Surfaces and Its Simulation Technology. *Comput. Geotech.* **2015**, *65*, 136–146. [CrossRef]
22. Srinivasa Rao, Y.; Reddy, T.V.K.; Nayudu, P.T. Groundwater Targeting in a Hard-Rock Terrain Using Fracture-Pattern Modeling, Niva River Basin, Andhra Pradesh, India. *Hydrogeol. J.* **2000**, *8*, 494–502. [CrossRef]
23. Su, X.; Feng, Y.; Chen, J.; Pan, J. The Characteristics and Origins of Cleat in Coal from Western North China. *Int. J. Coal Geol.* **2001**, *47*, 51–62. [CrossRef]
24. Gurov, E.P.; Koeberl, C. Shocked Rocks and Impact Glasses from the El'gygytgyn Impact Structure, Russia. *Meteorit. Planet. Sci.* **2004**, *39*, 1495–1508. [CrossRef]
25. Nascimento Da Silva, C.C.; De Medeiros, W.E.; De Sá, E.F.J.; Neto, P.X. Resistivity and Ground-Penetrating Radar Images of Fractures in a Crystalline Aquifer: A Case Study in Caiçara Farm—NE Brazil. *J. Appl. Geophys.* **2004**, *56*, 295–307. [CrossRef]
26. Watkins, H.; Butler, R.W.H.; Bond, C.E.; Healy, D. Influence of Structural Position on Fracture Networks in the Torridon Group, Achnashellach Fold and Thrust Belt, NW Scotland. *J. Struct. Geol.* **2015**, *74*, 64–80. [CrossRef]
27. Tsang, C.-F.; Bernier, F.; Davies, C. Geohydromechanical Processes in the Excavation Damaged Zone in Crystalline Rock, Rock Salt, and Indurated and Plastic Clays—In the Context of Radioactive Waste Disposal. *Int. J. Rock Mech. Min. Sci.* **2005**, *42*, 109–125. [CrossRef]
28. Goryainov, P.M.; Ivanyuk, G.Y.; Kalashnikov, A.O. Topography Formation as an Element of Lithospheric Self-Organization. *Russ. Geol. Geophys.* **2013**, *54*, 1071–1082. [CrossRef]

29. Ivanyuk, G.; Yakovenchuk, V.; Pakhomovsky, Y.; Kalashnikov, A.; Mikhailova, J.; Goryainov, P. *Self-Organization of the Khibiny Alkaline Massif (Kola Peninsula, Russia)*; InTech: Rijeka, Croatia, 2012.
30. Shevyrev, S.; Gorobeyko, E.V.; Carranza, E.J.M.; Boriskina, N.G. First-Pass Prospectivity Mapping for Au–Ag Mineralization in Sikhote–Alin Superterrane, Southeast Russia through Field Sampling, Image Enhancement on ASTER Data, and MaxEnt Modeling. *Earth Sci. Inform.* **2023**, *16*, 695–716. [CrossRef]
31. Jambayev, A.S. Discrete Fracture Network Modeling for a Carbonate Reservoir. Master's Thesis, Colorado School of Mines, Golden, CO, USA, 2013.
32. Panza, E.; Agosta, F.; Zambrano, M.; Tondi, E.; Prosser, G.; Giorgioni, M.; Janiseck, J.M. Structural Architecture and Discrete Fracture Network Modelling of Layered Fractured Carbonates (Altamura Fm., Italy). *Ital. J. Geosci.* **2015**, *134*, 409–422. [CrossRef]
33. Gauthier, B.D.M.; Lake, S.D. Probabilistic Modeling of Faults below the Limit of Seismic Resolution in Pelican Field, North Sea, Offshore United Kingdom. *Am. Assoc. Pet. Geol. Bull.* **1993**, *77*, 761–777. [CrossRef]
34. Nelson, R.A. *Geologic Analysis of Naturally Fractured Reservoirs*; Gulf Professional Publishing: Houston, TX, USA, 2001; p. 352, ISBN 9780884153177.
35. de Joussineau, G.; Aydin, A. The Evolution of the Damage Zone with Fault Growth in Sandstone and Its Multiscale Characteristics. *J. Geophys. Res. Solid Earth* **2007**, 112. [CrossRef]
36. Agosta, F.; Alessandroni, M.; Tondi, E.; Aydin, A. Oblique Normal Faulting along the Northern Edge of the Majella Anticline, Central Italy: Inferences on Hydrocarbon Migration and Accumulation. *J. Struct. Geol.* **2009**, *31*, 674–690. [CrossRef]
37. Agosta, F.; Tondi, E. Faulting and Fracturing of Carbonate Rocks: New Insights into Deformation Mechanisms, Petrophysics and Fluid Flow Properties. *J. Struct. Geol.* **2010**, *32*, 1185–1186. [CrossRef]
38. Rustichelli, A.; Tondi, E.; Agosta, F.; Cilona, A.; Giorgioni, M. Development and Distribution of Bed-Parallel Compaction Bands and Pressure Solution Seams in Carbonates (Bolognano Formation, Majella Mountain, Italy). *J. Struct. Geol.* **2012**, *37*, 181–199. [CrossRef]
39. Rustichelli, A.; Tondi, E.; Agosta, F.; Di Celma, C.; Giorgioni, M. Sedimentologic and Diagenetic Controls on Pore-Network Characteristics of Oligocene–Miocene Ramp Carbonates (Majella Mountain, Central Italy). *Am. Assoc. Pet. Geol. Bull.* **2013**, *97*, 487–524. [CrossRef]
40. Cacas, M.C.; Daniel, J.M.; Letouzey, J. Nested Geological Modelling of Naturally Fractured Reservoirs. *Pet. Geosci.* **2001**, *7*, S43–S52. [CrossRef]
41. Healy, D.; Rizzo, R.E.; Cornwell, D.G.; Farrell, N.J.C.; Watkins, H.; Timms, N.E.; Gomez-Rivas, E.; Smith, M. FracPaQ: A MATLAB^{TM} Toolbox for the Quantification of Fracture Patterns. *J. Struct. Geol.* **2017**, *95*, 1–16. [CrossRef]
42. Mace, R.E.; Marrett, R.A.; Hovorka, S.D. Fractal Scaling of Secondary Porosity in Karstic Exposures of the Edwards Aquifer. In Proceedings of the 10th Multidisciplinary Conference on Sinkholes and the Engineering and Environmental Impacts of Karst, San Antonio, TX, USA, 24–28 September 2005; Volume 40796, pp. 178–187. [CrossRef]
43. Verbovšek, T. Extrapolation of Fractal Dimensions of Natural Fracture Networks from One to Two Dimensions in Dolomites of Slovenia. *Geosci. J.* **2009**, *13*, 343–351. [CrossRef]
44. Bour, O.; Davy, P. Fault Length Distribution. *Water Resour.* **1997**, *33*, 1567–1583. [CrossRef]
45. Radliński, A.P.; Radlińska, E.Z.; Agamalian, M.; Wignall, G.D.; Lindner, P.; Randl, O.G. Fractal Geometry of Rocks. *Phys. Rev. Lett.* **1999**, *82*, 3078. [CrossRef]
46. Ehlen, J. Fractal Analysis of Joint Patterns in Granite. *Int. J. Rock Mech. Min. Sci.* **2000**, *37*, 909–922. [CrossRef]
47. Kusumayudha, S.B.; Zen, M.T.; Notosiswoyo, S.; Gautama, R.S. Fractal Analysis of the Oyo River, Cave Systems, and Topography of the Gunungsewu Karst Area, Central Java, Indonesia. *Hydrogeol. J.* **2000**, *8*, 271–278. [CrossRef]
48. Schuller, D.J.; Rao, A.R.; Jeong, G.D. Fractal Characteristics of Dense Stream Networks. *J. Hydrol.* **2001**, *243*, 1–16. [CrossRef]
49. Xiaohua, Z.; Yunlong, C.; Xiuchun, Y. On Fractal Dimensions of China's Coastlines. *Math. Geol.* **2004**, *36*, 447–461. [CrossRef]
50. Šušteršič, F. Relationships between Deflector Faults, Collapse Dolines and Collector Channel Formation: Some Examples from Slovenia. *Int. J. Speleol.* **2006**, *35*, 1–12. [CrossRef]
51. Brewer, J.; Di Girolamo, L. Limitations of Fractal Dimension Estimation Algorithms with Implications for Cloud Studies. *Atmos. Res.* **2006**, *82*, 433–454. [CrossRef]
52. Davy, P.; Bour, O.; De Dreuzy, J.-R.; Darcel, C. Flow in Multiscale Fractal Fracture Networks. *Geol. Soc. Lond. Spec. Publ.* **2006**, *261*, 31–45. [CrossRef]
53. Davy, P.; Le Goc, R.; Darcel, C.; Bour, O.; De Dreuzy, J.R.; Munier, R. A Likely Universal Model of Fracture Scaling and Its Consequence for Crustal Hydromechanics. *J. Geophys. Res. Solid Earth* **2010**, *115.*, 1–13. [CrossRef]
54. Verbovšek, T.; Veselič, M. Factors Influencing the Hydraulic Properties of Wells in Dolomite Aquifers of Slovenia. *Hydrogeol. J.* **2008**, *16*, 779–795. [CrossRef]
55. Lopes, R.; Betrouni, N. Fractal and Multifractal Analysis: A Review. *Med. Image Anal.* **2009**, *13*, 634–649. [CrossRef]
56. Liu, R.; Jiang, Y.; Li, B.; Wang, X. A Fractal Model for Characterizing Fluid Flow in Fractured Rock Masses Based on Randomly Distributed Rock Fracture Networks. *Comput. Geotech.* **2015**, *65*, 45–55. [CrossRef]
57. Pavičić, I.; Dragičević, I.; Vlahović, T.; Grgasović, T. Fractal Analysis of Fracture Systems in Upper Triassic Dolomites in Žumberak Mountain, Croatia. *Rud. Geol. Naft. Zb.* **2017**, *32*, 1–13. [CrossRef]
58. Mandelbrot, B. How Long Is the Coast of Britain? Statistical Self-Similarity and Fractional Dimension. *Science* **1967**, *156*, 636–638. [CrossRef]

59. Barker, J.A. A Generalized Radial Flow Model for Hydraulic Tests in Fractured Rock. *Water Resour. Res.* **1988**, *24*, 1796–1804. [CrossRef]
60. Turcotte, D.L. Fractals, Chaos, Self-organized Criticality and Tectonics. *Terra Nova* **1992**, *4*, 4–12. [CrossRef]
61. Turcotte, D. *Fractals and Chaos in Geology and Geophysics*, 2nd ed.; Cambridge University Press: Cambridge, UK, 1997; ISBN 9780521567336.
62. Rodriguez-Iturbe, I.; Rinaldo, A. *Fractal River Basins: Chance and Self-Organization*; Cambridge University Press: Cambridge, UK, 1997; ISBN 0521004055.
63. Boro, H.; Rosero, E.; Bertotti, G. Fracture-Network Analysis of the Latemar Platform (Northern Italy): Integrating Outcrop Studies to Constrain the Hydraulic Properties of Fractures in Reservoir Models. *Pet. Geosci.* **2014**, *20*, 79–92. [CrossRef]
64. Jacquemyn, C.; Huysmans, M.; Hunt, D.; Casini, G.; Swennen, R. Multi-Scale Three-Dimensional Distribution of Fracture- and Igneous Intrusion-Controlled Hydrothermal Dolomite from Digital Outcrop Model, Latemar Platform, Dolomites, Northern Italy. *Am. Assoc. Pet. Geol. Bull.* **2017**, *101*, 957–984. [CrossRef]
65. Mei, L.; Zhang, H.; Wang, L.; Zhang, Q.; Cai, J. Fractal Analysis of Shape Factor for Matrix-Fracture Transfer Function in Fractured Reservoirs. *Oil Gas Sci. Technol.* **2020**, *75*, 47. [CrossRef]
66. Barton, C.C. Fractal Analysis of Scaling and Spatial Clustering of Fractures. In *Fractals in the Earth Sciences*; Springer: Boston, MA, USA, 1995; pp. 141–178.
67. Zetterlund, M.; Ericsson, L.O.; Stigsson, M. Fracture Mapping for Geological Prognoses. Comparison of Fractures from Boreholes, Tunnel and 3-D Blocks. In Proceedings of the ISRM International Symposium—EUROCK 2012, Stockholm, Sweden, 28–30 May 2012; pp. 1–13.
68. Lee, C.-C.; Lee, C.-H.; Yeh, H.-F.; Lin, H.-I. Modeling Spatial Fracture Intensity as a Control on Flow in Fractured Rock. *Environ. Earth Sci.* **2011**, *63*, 1199–1211. [CrossRef]
69. Ukar, E.; Laubach, S.E.; Hooker, J.N. Outcrops as Guides to Subsurface Natural Fractures: Example from the Nikanassin Formation Tight-Gas Sandstone, Grande Cache, Alberta Foothills, Canada. *Mar. Pet. Geol.* **2019**, *103*, 255–275. [CrossRef]
70. Pan, J.B.; Lee, C.C.; Lee, C.H.; Yeh, H.F.; Lin, H.I. Application of Fracture Network Model with Crack Permeability Tensor on Flow and Transport in Fractured Rock. *Eng. Geol.* **2010**, *116*, 166–177. [CrossRef]
71. Jelmert, T.A. Fractal Dimensions of a Fractured Formation in the Rondane Mountain Plateau, Norway. In Proceedings of the IAMG'05: GIS and Spatial Analysis, Toronto, ON, Canada, 21–26 August 2005; Volume 1, pp. 329–334.
72. Park, S.I.; Kim, Y.S.; Ryoo, C.R.; Sanderson, D.J. Fractal Analysis of the Evolution of a Fracture Network in a Granite Outcrop, SE Korea. *Geosci. J.* **2010**, *14*, 201–215. [CrossRef]
73. Watanabe, K.; Takahashi, H. Fractal Characterization of Subsurface Fracture Network for Geothermal Energy Extraction System. In Proceedings of the 18th Workshop on Geothermal Reservoir Engineering Stanford University, Stanford, CA, USA, 26–28 January 1993; pp. 119–124.
74. Gurel, E.; Coskuner, Y.B.; Akin, S. Fractal Modeling of Outcrop Fracture Patterns in Alasehir Geothermal Reservoir Turkey. In Proceedings of the 41st Workshop on Geothermal Reservoir Engineering, Stanford, CA, USA, 22–24 February 2016; pp. 1–8.
75. Yao, Y.; Wu, Y.S.; Zhang, R. The Transient Flow Analysis of Fluid in a Fractal, Double-Porosity Reservoir. *Transp. Porous Media* **2012**, *94*, 175–187. [CrossRef]
76. Xu, P.; Liu, H.; Sasmito, A.P.; Qiu, S.; Li, C. Effective Permeability of Fractured Porous MEDIA with FRACTAL DUAL-POROSITY MODEL. *Fractals* **2017**, *25*, 1740014. [CrossRef]
77. Wang, W.; Yuan, B.; Su, Y.; Sheng, G.; Yao, W.; Gao, H.; Wang, K. A Composite Dual-Porosity Fractal Model for Channel-Fractured Horizontal Wells. *Eng. Appl. Comput. Fluid Mech.* **2018**, *12*, 104–116. [CrossRef]
78. Bolshov, L.; Kondratenko, P.; Matveev, L.; Pruess, K. Elements of Fractal Generalization of Dual-Porosity Model for Solute Transport in Unsaturated Fractured Rocks. *Vadose Zone J.* **2008**, *7*, 1198–1206. [CrossRef]
79. Kim, T.H.; Schechter, D.S. Estimation of Fracture Porosity of Naturally Fractured Reservoirs With No Matrix Porosity Using Fractal Discrete Fracture Networks. *SPE Reserv. Eval. Eng.* **2009**, *12*, 232–242. [CrossRef]
80. Díaz, E. Evaluation of a Discrete Fracture Network (DFN) Model and Comparison with Fractured Carbonate Outcrops, Monte Conero, Italy. In Proceedings of the 7th European Congress on Regional Geoscientific Cartography and Information Systems, Bologna, Italy, 12–15 June 2012.
81. Bisdom, K.; Gauthier, B.D.M.; Bertotti, G.; Hardebol, N.J. Calibrating Discrete Fracture-Network Models with a Carbonate Three-Dimensional Outcrop Fracture Network: Implications for Naturally Fractured Reservoir Modeling. *Am. Assoc. Pet. Geol. Bull.* **2014**, *98*, 1351–1376. [CrossRef]
82. Cacas, M.C.; Ledoux, E.; de Marsily, G.; Tillie, B.; Barbreau, A.; Durand, E.; Feuga, B.; Peaudecerf, P. Modeling Fracture Flow with a Stochastic Discrete Fracture Network: Calibration and Validation: 1. *The Flow Model. Water Resour. Res.* **1990**, *26*, 479–489. [CrossRef]
83. Voeckler, H.; Allen, D.M. Estimating Regional-Scale Fractured Bedrock Hydraulic Conductivity Using Discrete Fracture Network (DFN) Modeling. *Hydrogeol. J.* **2012**, *20*, 1081–1100. [CrossRef]
84. Lei, Q.; Latham, J.-P.; Tsang, C.-F. The Use of Discrete Fracture Networks for Modelling Coupled Geomechanical and Hydrological Behaviour of Fractured Rocks. *Comput. Geotech.* **2017**, *85*, 151–176. [CrossRef]
85. Bearinger, D.; Hillier, C. Fracture Characterization: From Core to Discrete Fracture Network Model. *Geophysics* **2016**, *39*, 347–383.

86. Tavakkoli, M.; Mohammadsadeghi, M.; Shaheabadi, A.; Khajoee, S.; Malakooti, R.; Beidokhti, M.S. Deterministic versus Stochastic Discrete Fracture Network (DFN) Modeling, Application in a Heterogeneous Naturally Fractured Reservoir. In Proceedings of the Kuwait International Petroleum Conference and Exhibition, Kuwait City, Kuwait, 14–16 December 2009. [CrossRef]
87. Zambrano, M.; Tondi, E.; Korneva, I.; Panza, E.; Agosta, F.; Janiseck, J.M.; Giorgioni, M. Fracture Properties Analysis and Discrete Fracture Network Modelling of Faulted Tight Limestones, Murge Plateau, Italy. *Ital. J. Geosci.* **2016**, *135*, 55–67. [CrossRef]
88. Panza, E.; Sessa, E.; Agosta, F.; Giorgioni, M. Discrete Fracture Network Modelling of a Hydrocarbon-Bearing, Oblique-Slip Fault Zone: Inferences on Fault-Controlled Fluid Storage and Migration Properties of Carbonate Fault Damage Zones. *Mar. Pet. Geol.* **2018**, *89*, 263–279. [CrossRef]
89. Pavičić, I. *Origin, Spatial Distribution and Qunatification of Porosity in Upper Triassic Dolomites in Žumberak Mts*; University of Zagreb: Zagreb, Croatia, 2018.
90. Grgasović, T. *Stratigraphy of Later Triassic Deposits in Žumberak Area*; Faculty of Scinece, University of Zagreb: Zagreb, Croatia, 1998.
91. von Gümbel, C.W. Geognostische Mittheilungen Aus Den Alpen, Das Mendel-Und Schlerngebirge. Sitzungsberichte der Bayer. *Akad. der Wiss. Math.-Phys. Cl.* **1873**, *1873*, 14–88.
92. Ichiki, M.; Ogawa, Y.; Kaida, T.; Koyama, T.; Uyeshima, M.; Demachi, T.; Hirahara, S.; Honkura, Y.; Kanda, W.; Kono, T.; et al. Electrical image of subduction zone beneath northeastern Japan. *J. Geophys. Res. Solid Earth* **2015**, *120*, 7937–7965. [CrossRef]
93. Doglioni, C. Tectonics of the Dolomites (Southern Alps, Northern Italy). *J. Struct. Geol.* **1987**, *9*, 181–193. [CrossRef]
94. Masaryk, P.; Lintnerová, O. Diagenesis and Porosity of the Upper Triassic Carbonates of the Pre-Neogene Vienna Basin Basement. *Geol. Carpathica* **1997**, *48*, 371–386.
95. Haas, J.; Budai, T. Triassic Sequence Stratigraphy of the Transdanubian Range (Hungary). *Geol. Carpathica* **1999**, *50*, 459–475.
96. Haas, J. Facies Analysis of the Cyclic Dachstein Limestone Formation (Upper Triassic) in the Bakony Mountains, Hungary. *Facies* **2004**, *50*, 263–286. [CrossRef]
97. Schleicher, D. Hausdorff Dimension, Its Properties, and Its Surprises. *Am. Math. Mon.* **2007**, *114*, 509–528. [CrossRef]
98. Mandelbrot, B.B. *The Fractal Geometry of Nature/Revised and Enlarged Edition*; WH Free Co.: New York, NY, USA, 1983; Volume 1495.
99. Falconer, K. *Fractal Geometry: Mathematical Foundations and Applications*; John Wiley & Sons: Hoboken, NJ, USA, 2013; Volume 53, ISBN 9788578110796.
100. Barton, C.C.; Paul, R.; Pointe, L. *Fractals in the Earth Sciences*; Plenum Press: New York, NY, USA, 1995; Volume 53, ISBN 978-1-4899-1399-9.
101. Steacy, S.J.; Sammis, C.G. An Automaton for Fractal Patterns of Fragmentation. *Nature* **1991**, *353*, 250–252. [CrossRef]
102. Baveye, P.; Boast, C.W.; Ogawa, S.; Parlange, J.Y.; Steenhuis, T. Influence of Image Resolution and Thresholding on the Apparent Mass Fractal Characteristics of Preferential Flow Patterns in Field Soils. *Water Resour. Res.* **1998**, *34*, 2783–2796. [CrossRef]
103. Wang, W. Rock Fracture Image Segmentation Algorithms. In *Image Segmentation*; InTech: London, UK, 2011.
104. Yu, B.M. Fractal Dimensions for Multiphase Fractal Media. *Fractals* **2006**, *14*, 111–118. [CrossRef]
105. Leonard, T.; Papasouliotis, O.; Main, I.G. A Poisson Model for Identifying Characteristic Size Effects in Frequency Data: Application to Frequency-size Distributions for Global Earthquakes,"Starquakes", and Fault Lengths. *J. Geophys. Res. Solid Earth* **2001**, *106*, 13473–13484. [CrossRef]
106. Karperien, A. *Fraclac for Imagej*; Charles Sturt University: Bathurst, Australia, 2013.
107. La Pointe, P.R. A Method to Characterize Fracture Density and Connectivity through Fractal Geometry. *Int. J. Rock Mech. Min. Sci. Geomech. Abstr.* **1988**, *25*, 421–429. [CrossRef]
108. Verbovšek, T. Hydrogeology and Geochemistry of Fractured Dolomites—A Case Study of Slovenia. In *Aquifers: Formation, Transport and Pollution*; Laughton, R.H., Ed.; Nova Science Publishers, Inc.: New York, NY, USA, 2009; ISBN 978-1-61668-051-0.
109. Billi, A.; Salvini, F.; Storti, F. The Damage Zone-Fault Core Transition in Carbonate Rocks: Implications for Fault Growth, Structure and Permeability. *J. Struct. Geol.* **2003**, *25*, 1779–1794. [CrossRef]
110. Fisher, Q.J.; Knipe, R.J. The Permeability of Faults within Siliciclastic Petroleum Reservoirs of the North Sea and Norwegian Continental Shelf. *Mar. Pet. Geol.* **2001**, *18*, 1063–1081. [CrossRef]
111. Antonellini, M.; Aydin, A. Effect of Faulting on Fluid Flow in Porous Sandstones: Geometry and Spatial Distribution. *Am. Assoc. Pet. Geol. Bull.* **1995**, *79*, 642–671.
112. Storti, F.; Balsamo, F.; Cappanera, F.; Tosi, G. Sub-Seismic Scale Fracture Pattern and in Situ Permeability Data in the Chalk atop of the Krempe Salt Ridge at Lägerdorf, NW Germany: Inferences on Synfolding Stress Field Evolution and Its Impact on Fracture Connectivity. *Mar. Pet. Geol.* **2011**, *28*, 1315–1332. [CrossRef]
113. Wennberg, O.P.; Svånå, T.; Azizzadeh, M.; Aqrawi, A.M.M.; Brockbank, P.; Lyslo, K.B.; Ogilvie, S. Fracture Intensity vs. Mechanical Stratigraphy in Platform Top Carbonates: The Aquitanian of the Asmari Formation, Khaviz Anticline, Zagros, SW Iran. *Pet. Geosci.* **2006**, *12*, 235–245. [CrossRef]